Journal of Materials Chemistry C

PAPER

View Article Online
View Journal | View Issue

Cite this: J. Mater. Chem. C, 2015, 3, 5307

Composition and bandgap control of $Al_xGa_{1-x}N$ films synthesized by plasma-assisted pulsed laser deposition†

Hua Cai,[ab] Peipei Liang,[a] René Hübner,[b] Shengqiang Zhou,[b] Yanli Li,[a] Jian Sun,[a] Ning Xu[a] and Jiada Wu*[a]

Received 17th February 2015,
Accepted 20th April 2015

DOI: 10.1039/c5tc00475f

www.rsc.org/MaterialsC

Ternary $Al_xGa_{1-x}N$ films with different Al compositions were synthesized on sapphire and Si substrates by pulsed laser co-ablation of a polycrystalline GaAs target and a metallic Al target in nitrogen plasma generated by electron cyclotron resonance discharge of N_2 gas. Spectroscopy was used to characterize the synthesis process for the mechanisms responsible for $Al_xGa_{1-x}N$ synthesis and film deposition. The synthesized $Al_xGa_{1-x}N$ films were evaluated using field emission scanning electron microscopy, atomic force microscopy, X-ray diffraction, Fourier-transform infrared spectroscopy, Raman scattering spectroscopy, transmission electron microscopy and optical transmission measurements. The $Al_xGa_{1-x}N$ films have hexagonal wurtzite structure, which degenerates as the Al composition increases, and show high optical transparency with the absorption edge blue shifted and the bandgap widened with the increasing Al composition. A comparison of the synthesized $Al_xGa_{1-x}N$ films with the binary GaN and AlN films synthesized by a similar method reveals their similarity in the structure and the optical properties.

1. Introduction

Successful applications of direct bandgap semiconducting III-nitrides in optoelectronics and integrated circuits are largely attributed to the capability of energy-band engineering through composition regulation.[1,2] Ternary $Al_xGa_{1-x}N$ and $In_xGa_{1-x}N$ alloys have tunable direct bandgaps from 0.75 eV (InN) to 6.2 eV (AlN).[3,4] Their superior properties have been demonstrated in light emission covering the spectral region ranging from infrared (IR) to ultraviolet (UV), excellent thermal conductivity and hardness and high resistance to chemicals, which make the III-nitrides promising for potential applications in light-emitting diodes,[2,5] photodetectors and field effect transistors.[6–8] To date, $Al_xGa_{1-x}N$ alloys can be synthesized by various methods including metal–organic chemical vapor deposition (MOCVD)[9,10] and molecular beam epitaxy (MBE).[11–13] For most methods, however, a high growth temperature is usually required, which will induce undesirable effects such as thermal strains and defects in the grown films, chemical reactions at the interfaces, as well as the deterioration of substrates or pre-buried layers. Therefore, approaches employing lower growth temperatures are preferred. In addition, the composition regulation of ternary $Al_xGa_{1-x}N$ systems has been a rather tough issue so far. When using MOCVD or MBE, for example, it is usually difficult in getting appropriate partial pressures of Al- and Ga-containing sources to synthesize $Al_xGa_{1-x}N$ with controllable compositions.

Pulsed laser deposition (PLD) has been established as a versatile technique for preparing various thin films.[14,15] It is possible to reduce the growth temperature by means of this technique, since the average energy of the laser ablated species is considerably high. It is also convenient to control the quantity of target material transferred to the growing film by adjusting the laser energy density or the pulse repetition rate. When PLD is performed in a reactive gaseous environment, in addition, the ablated species undergo a reactive expansion, and hence compound films can be synthesized through reactive deposition. PLD can also be combined with other techniques or assisted by other sources such as plasma and ion beams, forming PLD-based hybrid methods.[14] In particular, reactive plasmas composed of multiple reactive species are very effective to assist reactive synthesis of various materials in a broad range of composition, structure and dimensionality.[14,16,17] The epitaxial growth of GaN films has been achieved by laser ablation of the Ga target in a radio-frequency plasma ambient.[18] The same group also reported the growth of high quality AlN films by PLD assisted with nitrogen plasma.[19]

We have previously demonstrated an alternative approach to the low-temperature synthesis of high Al composition ternary

[a] Department of Optical Science and Engineering, Fudan University, Shanghai 200433, China. E-mail: jdwu@fudan.edu.cn; Fax: +86 21 55664529; Tel: +86 21 65642150
[b] Institute of Ion Beam Physics and Materials Research, Helmholtz-Zentrum Dresden-Rossendorf, P.O. Box 510119, 01314 Dresden, Germany

† CCDC 1040176 and 1040177. For crystallographic data in CIF or other electronic format see DOI: 10.1039/c5tc00475f

$Al_xGa_{1-x}N$ by pulsed laser co-ablation of a polycrystalline GaAs target and a metallic Al target with the assistance of nitrogen plasma generated by electron cyclotron resonance (ECR) microwave discharge of N_2 gas.[20] In the present work, the variation of the Al composition in $Al_xGa_{1-x}N$ and hence the bandgap modulation of $Al_xGa_{1-x}N$ were realized by simply varying the repetition rate of the laser pulses ablating the Al target. Compositional analysis, structural characterization and optical measurements were performed for the synthesized $Al_xGa_{1-x}N$ films having varied Al composition x and were compared with the corresponding characteristics of binary AlN (x = 1) and GaN (x = 0) films synthesized by single target ablation of Al or GaAs. The synthesis process was spectroscopically characterized by monitoring and analyzing the optical emission from the plasma formed during the synthesis of $Al_xGa_{1-x}N$ and the mechanisms responsible for the preparation of $Al_xGa_{1-x}N$ films were discussed.

2. Experimental details

2.1 Sample preparation

The equipment and the method used for sample preparation have been described previously,[20] except that the two laser beams were delivered using two frequency-doubled Q-switched Nd:YAG lasers which were controlled separately in the present work. In the environment of nitrogen plasma generated by ECR microwave discharge of pure (99.999%) N_2 gas using a 2.45 GHz microwave, a polycrystalline GaAs target and a metallic Al target were ablated simultaneously using two focused laser beams (wavelength: 532 nm; pulse width: 5 ns). The laser beams were incident on the target surfaces at an angle of 45° with a spot size of about 1 mm^2 and a laser fluence of about 3 J cm^{-2}. The laser used for GaAs ablation worked at a constant repetition rate of 10 Hz, while the repetition rate of the other laser for Al ablation could be adjusted from 1 to 10 Hz, providing a varied amount of Al for the growing film and hence synthesizing ternary $Al_xGa_{1-x}N$ films having different Al compositions with the assistance of the nitrogen plasma. Binary GaN and AlN films were also synthesized when one of the laser beams was blocked and only the GaAs target or the Al target was ablated using a pulsed laser beam with a 10 Hz repetition rate. Polished Si(100) wafers and double side polished *c*-plane sapphire wafers were used as the substrates after being carefully cleaned and placed 45 mm away from the laser-irradiated spots. The surface of sapphire plates was first nitridized by irradiating with the nitrogen plasma stream for 5 min prior to film deposition. All films were deposited for 1 hour. The deposited films were annealed at 800 °C in a flowing N_2 atmosphere ($\sim 10^5$ Pa) for 1 hour.

In this paper, the annealed GaN film deposited by ablating the GaAs target, the annealed $Al_xGa_{1-x}N$ films deposited by co-ablating the GaAs and Al targets with the laser ablating the Al target working at 1, 5 and 10 Hz, and the annealed AlN film deposited by ablating the Al target are denoted as samples A, B, C, D and E, respectively.

2.2 Optical emission measurements

For the spectroscopic study on the process of $Al_xGa_{1-x}N$ synthesis, optical emission of the plasmas generated by ECR discharge and pulsed laser ablation was monitored. The plasmas were imaged onto an UV-Vis optical fiber bundle (Acton Research, ILG-455-020-1) using a light collecting lens. The optical emission of the plasmas was transmitted to the entrance slit of a 0.5 m spectrometer (Acton Research, Spectra Pro 500i), resolved using the spectrometer and recorded using a gated intensified charge coupled device (ICCD) (Princeton Instruments, PI-Max 1KRB-FG-43) which was mounted on the exit port of the spectrometer. Time-integrated spectra were recorded by accumulating 100 times with a gate width of 6 μs.

2.3 Sample characterization

The sample morphology was examined by field emission scanning electron microscopy (FESEM) using a Hitachi S-4800 microscope and atomic force microscopy (AFM) using a Shimadz SPM-950013 scanning probe microscope working in the AFM dynamic mode. The sample composition was determined by energy dispersive X-ray spectroscopy (EDXS) using a Philips XL30FEG* SEM operating at an accelerating voltage of 30 kV and equipped with an EDAX EDX detector. The sample structure was characterized by X-ray diffraction (XRD) using a Rigaku D/max-γ B X-ray diffractometer with a rotating anode operating at 40 kV and 300 mA and Ni-filtered Cu Kα radiation (λ = 0.15406 nm). The structure was also characterized through the analysis of vibration modes by means of Fourier-transform infrared (FTIR) spectroscopy and Raman backscattering spectroscopy. FTIR measurements were carried out using a Nicolet Nexus 470 spectrometer. Raman measurements were performed using a Jobin-Yvon HR-Evolution confocal micro-Raman spectrometer with a 325 nm He–Cd laser beam for efficient resonance excitation of the samples. The transmission spectra were recorded for the films deposited on sapphire substrates using an ultraviolet-near infrared (UV-near IR) spectrophotometer (UV-3000, Hitachi) for optical characterization.

To locally analyze the microstructure of the synthesized films, transmission electron microscopy (TEM) investigations were performed using an image-corrected Titan 80-300 microscope (FEI) at an accelerating voltage of 300 kV. Besides bright-field TEM imaging at medium magnification and high-resolution TEM at enhanced magnification, selected area electron diffraction (SAED) was used to characterize the microstructure of the films. Since the smallest available selected area aperture of 10 μm covers a circular area with a diameter of about 190 nm, glue may contribute to the SAED patterns recorded. Prior to each TEM analysis, the specimen mounted in a double tilt analytical holder was placed for 10 s into a Model 1020 Plasma Cleaner (Fischione) to remove organic contamination. Classical cross-sectional TEM specimens were prepared by sawing, grinding, dimpling, and final Ar ion milling.

3. Results and discussion

3.1 Plasma emission and $Al_xGa_{1-x}N$ synthesis

ECR discharge of the working N_2 gas resulted in the activation of the N_2 gas and the formation of a reactive nitrogen plasma containing highly excited nitrogen species including nitrogen molecules and molecular ions.[21,22] The ablation of the Al and

GaAs targets generated an aluminum plume containing energetic aluminum atoms and atomic ions ablated from the Al target and a gallium–arsenic plume containing energetic gallium and arsenic atoms and atomic ions ablated from the GaAs target. The presence of excited nitrogen molecules and molecular ions, energetic aluminum, gallium and arsenic atoms and atomic ions is confirmed by optical emission measurements.

Fig. 1 illustrates a typical time-integrated spectrum taken from the plasma generated by the ECR discharge of N_2 gas and co-ablation of the Al and GaAs targets using two synchronized 10 Hz pulsed laser beams. In addition to the emission lines from monoatomic aluminum, gallium and arsenic atoms and atomic ions, the emission bands of diatomic nitrogen molecules and molecular ions are clearly resolved in the spectrum, indicating that the nitrogen gas was highly excited. The high-resolution spectra in the insets of Fig. 1 show the fine structures of the emission bands of diatomic nitrogen molecular ions and the emission lines of monoatomic atoms and ions. Nitrogen was first excited by ECR discharge, and its excitation was further enhanced by the fast expansion of the ablation plumes.[22] The ablation plumes underwent a highly reactive expansion in the reactive environment of the nitrogen plasma. During their travel in the reactive nitrogen plasma, the energetic ablated target species reacted with the excited nitrogen species at high rates, forming gaseous nitride precursors. Meanwhile, the surface of the substrate as well as the growing film was concurrently bombarded by the low-energy nitrogen plasma stream, enhancing the reactions between the reactive nitrogen species and the ablated target species arriving at the film surface.

From a thermodynamic point of view, AlN and GaN are more stable than arsenic nitrides, the reactive nitrogen species are thus expected to react preferentially with aluminum and gallium.[23] Moreover, the negative enthalpies for the formation of AlN and GaN are higher than that of GaAs.[24,25] Therefore, the aluminum and gallium atoms and ions in the plumes reacted exclusively with the reactive nitrogen species present in the nitrogen plasma at high rates, forming $Al_xGa_{1-x}N$ precursors for $Al_xGa_{1-x}N$ film deposition. In addition, the bombardment of the film surface by the nitrogen plasma stream also induced the breaking of the Ga–As bonds adsorbed on the surface, as in the case of plasma nitridation of the GaAs surface for GaN formation.[23] As a result, arsenic was excluded in the synthesis of $Al_xGa_{1-x}N$ films, a situation somewhat similar to the deposition of GaN films by reactive sputtering the GaAs target,[24] or by laser ablating the GaAs target in nitrogen plasma.[26]

3.2 Morphology and composition

The synthesized $Al_xGa_{1-x}N$ films including GaN ($x = 0$) and AlN ($x = 1$) films deposited on Si and sapphire substrates show a smooth surface appearance and are stable and adherent to the substrates. Fig. 2 shows the overview and cross-sectional FESEM images of samples A, D and E grown on Si substrates. The sample surface is rather smooth except a few particles randomly distributed on it. The cross-sectional FESEM images reveal that the synthesized films have a dense structure. The ternary $Al_xGa_{1-x}N$ films synthesized by 1, 5 and 10 Hz ablation of the Al target have thicknesses of about 110, 150 and 190 nm, while the binary GaN and AlN films are 100 and 85 nm in thickness, respectively. AFM observation also reveals the smooth surface of the synthesized

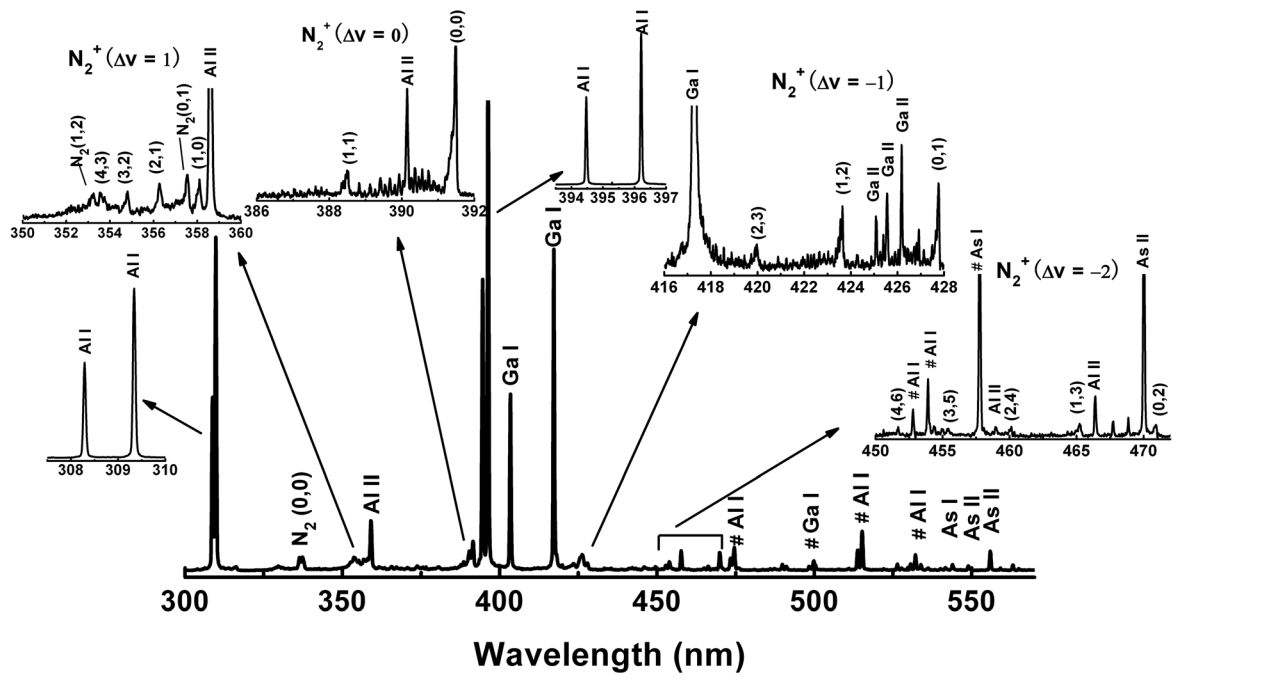

Fig. 1 Time-integrated spectrum of the optical emission of the plasmas generated by ECR discharge of N_2 and co-ablation of Al and GaAs targets during $Al_xGa_{1-x}N$ synthesis. The insets show high-resolution spectra of nitrogen molecular ions and aluminum, gallium and arsenic atoms and atomic ions. The lines marked by # are the second order diffractions of corresponding atomic emission lines.

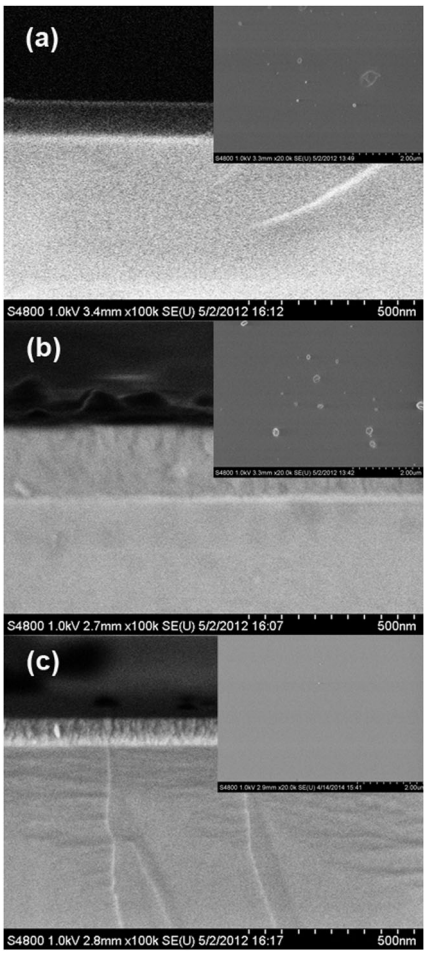

Fig. 2 Cross-sectional SEM images and overview SEM images (insets) of synthesized samples A (a), D (b) and E (c).

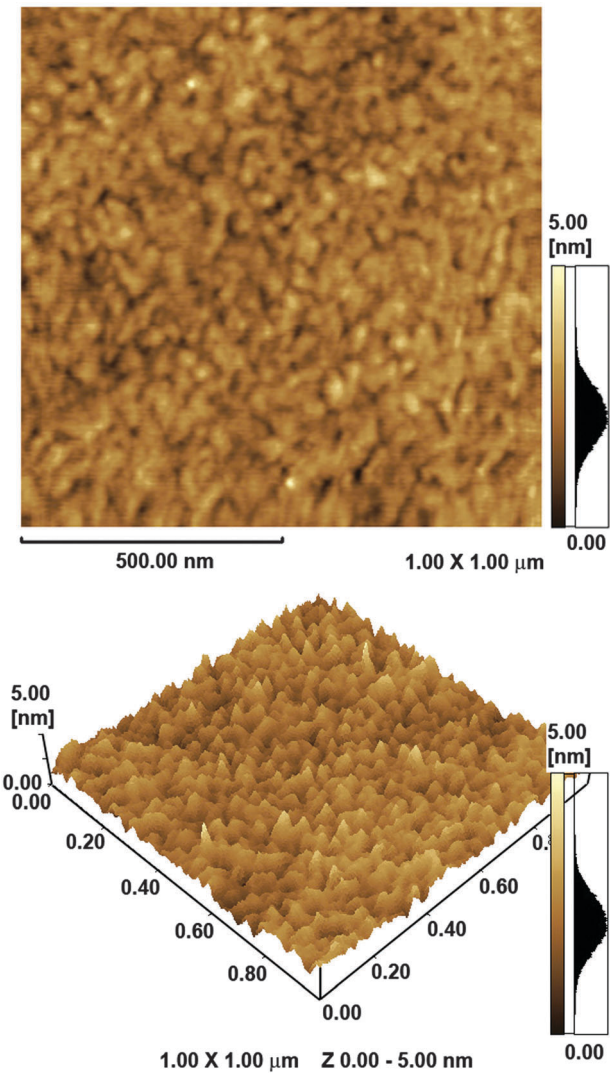

Fig. 3 AFM images of sample D.

films and gives root mean square (RMS) values of surface roughness in the range between 0.8 and 1.0 nm over the 1 μm × 1 μm area for the as-grown films, whereas the average RMS value of the annealed films slightly increases to about 1.5 nm. As representatives, typical AFM images taken from sample D are shown in Fig. 3.

The EDXS patterns of the films deposited on Si substrates are shown in Fig. 4, from which the Al compositions in $Al_xGa_{1-x}N$ samples B, C and D were determined to be about 0.14, 0.27 and 0.57, respectively, as shown in the inset of Fig. 4. The synthesized $Al_xGa_{1-x}N$ films are slightly rich in N with about 52 at% of nitrogen. It is also found that the AlN and GaN films are also non-stoichiometric and slightly nitrogen rich. In addition, the method was demonstrated to be capable of synthesizing $Al_xGa_{1-x}N$ films with different Al compositions by simply changing the repetition rate of laser ablating the Al target. The Al composition in $Al_xGa_{1-x}N$ can also be adjusted by varying the laser fluence on the Al target.[20]

3.3 Structure

Fig. 5 illustrates the XRD patterns taken from $Al_xGa_{1-x}N$ films B, C and D together with those from the GaN and AlN films.

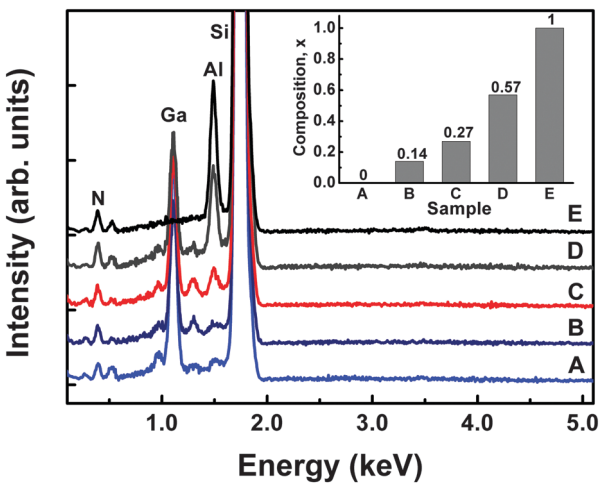

Fig. 4 EDXS patterns of synthesized samples A (A), B (B), C (C), D (D), and E (E). The inset shows Al compositions of these samples.

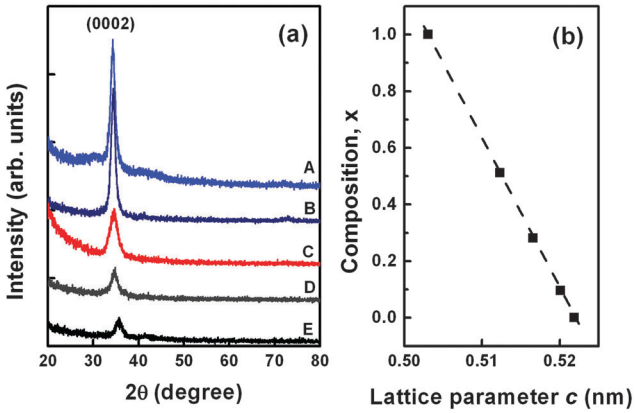

Fig. 5 (a) XRD patterns of samples A (A), B (B), C (C), D (D), and E (E) synthesized on sapphire substrates. (b) The correlation between lattice parameter c and Al composition x.

A prominent diffraction peak is clearly resolved in each pattern. For $Al_xGa_{1-x}N$ films B, C and D, this peak appears at $2\theta = 34.46$, 34.70 and 35.00°, respectively, while for GaN and AlN films the diffractions peak at $2\theta = 34.32$ and 35.66°. They can be indexed to the (0002) diffraction of wurtzite $Al_xGa_{1-x}N$, GaN and AlN, respectively, indicating the hexagonal wurtzite structure with c-axis oriented growth of the films. The singlet of the (0002) diffraction in the XRD patterns recorded from the $Al_xGa_{1-x}N$ films reveals the single-phase ternary alloys. The shift of the diffraction peak position is attributed to the variation in the lattice due to different Al compositions in the films. From the XRD data, the lattice parameters of films A, B, C, D and E were determined to be $c_A = 0.5222$ nm, $c_B = 0.5201$ nm, $c_C = 0.5166$ nm, $c_D = 0.5123$ nm and $c_E = 0.5031$ nm, respectively. The lattice parameter c of ternary $Al_xGa_{1-x}N$ with Al composition x can be related to those of binary AlN and GaN according to Vegard's law,[27–29]

$$c_{Al_xGa_{1-x}N} = xc_{AlN} + (1 - x)c_{GaN} \quad (1)$$

The Al compositions in $Al_xGa_{1-x}N$ films B, C, and D were thus determined to be 0.11, 0.29 and 0.52, respectively, consistent with the EDXS results. It also seems that the incorporation of Al results in the degradation of the crystal structure, as suggested by the reduction in the diffraction intensity and the broadening in the diffraction width.

Fig. 6 shows the FTIR transmission spectra of the samples synthesized on Si substrates. The spectra in Fig. 6 have been background corrected for the Si substrate and only weak absorption attributed to the Si–O–Si stretching vibration remains near 1100 cm^{-1}. It can be seen that the principle IR absorptions of the GaN and AlN films appear at about 556 and 680 cm^{-1}, respectively. The former absorption is attributed to the E_1 symmetry with transverse-optical (TO) phonons E_1(TO) of wurtzite GaN[30,31] and the latter one to that of wurtzite AlN.[30–33] The characteristic absorptions of hexagonal wurtzite GaN and AlN confirm the hexagonal wurtzite structure of the GaN and AlN films. The ternary $Al_xGa_{1-x}N$ films have higher frequencies of absorption assigned to the E_1(TO) mode than the GaN film has, with blue

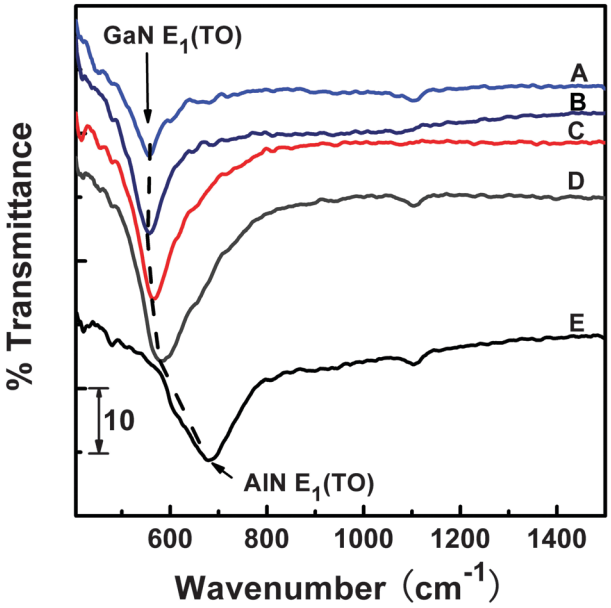

Fig. 6 FTIR spectra of samples A (A), B (B), C (C), D (D), and E (E) synthesized on Si substrates.

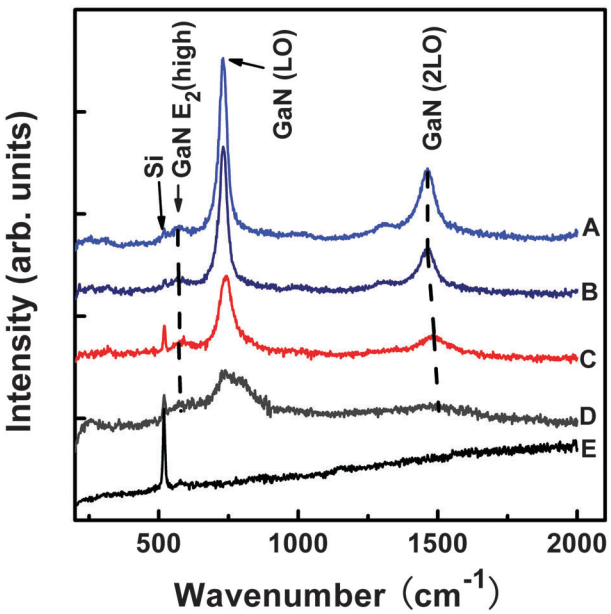

Fig. 7 Raman scattering spectra of samples A (A), B (B), C (C), D (D), and E (E) on Si substrates excited by 325 nm laser light.

shifts of about 2, 12 and 24 cm^{-1}, respectively, for samples B, C, and D compared with E_1(TO) absorption of the GaN film. The blue shift in the characteristic IR absorption could be associated with the increase of Al composition in $Al_xGa_{1-x}N$.[34] Therefore, the FTIR analysis indicates that the synthesized ternary $Al_xGa_{1-x}N$ films exhibit the IR features of the single ternary $Al_xGa_{1-x}N$ phase.

Raman scattering measurements provide another evidence for the hexagonal wurtzite structure and the single phase of the synthesized $Al_xGa_{1-x}N$ films. Hexagonal wurtzite structure has

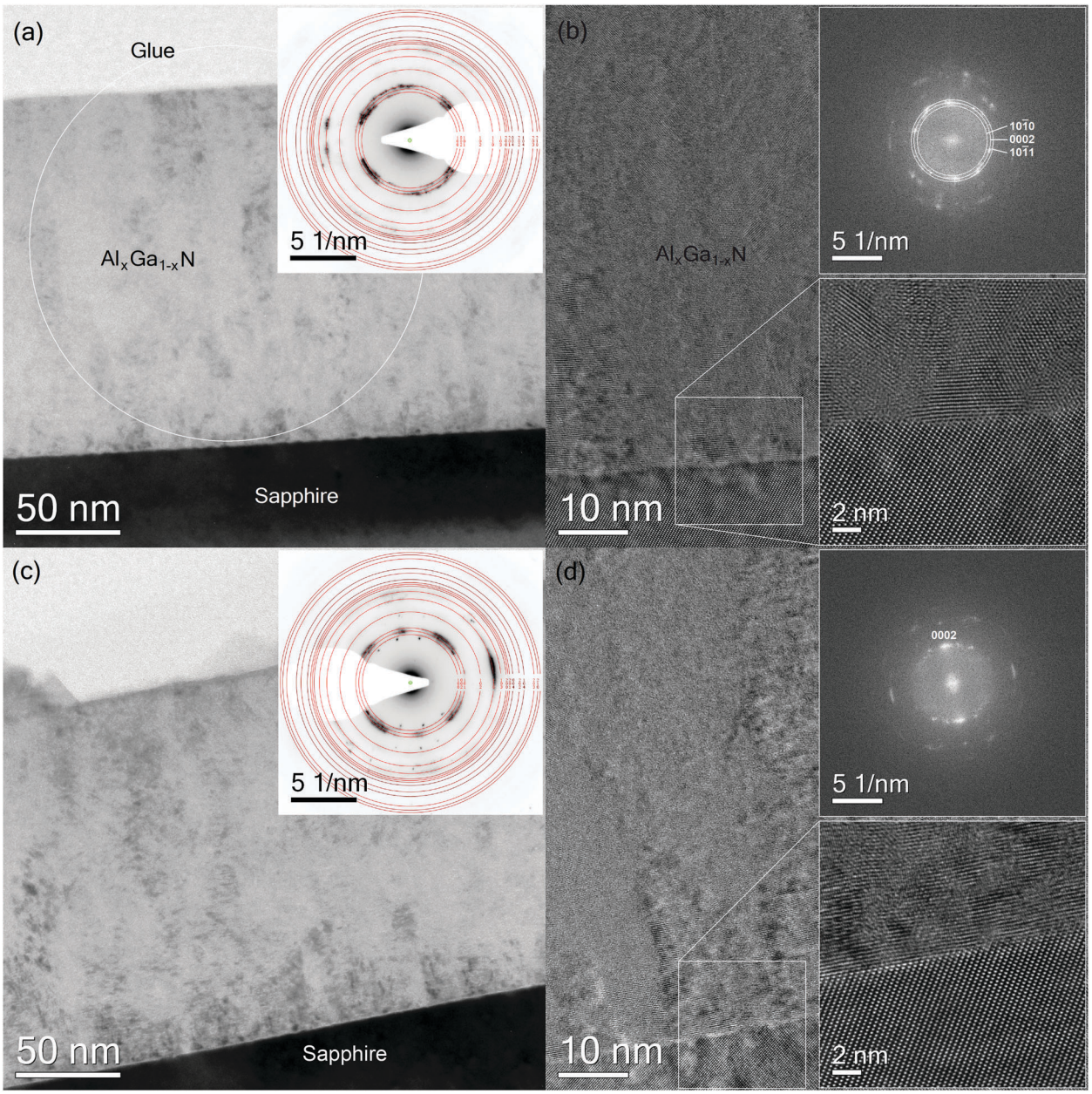

Fig. 8 (a) and (c) show cross-sectional bright-field TEM micrographs of the as-grown and annealed $Al_xGa_{1-x}N$ (sample D) films on the sapphire substrate, respectively. The insets show representative SAED patterns of the corresponding films. In particular, a circular area with 190 nm diameter as indicated by the white circle was used for SAED. (b) and (d) show cross-sectional high-resolution TEM images of the film-sapphire substrate interface region for the as-grown and annealed $Al_xGa_{1-x}N$ films, respectively. The upper right insets show Fourier transformations of the film obtained near the interface of the substrate. The lower right insets enlarge the film-substrate interface.

six Raman active phonon modes.[30,33,35,36] The Raman modes of GaN can be efficiently excited by 325 nm laser light whose photon energy is resonant with the electronic interband transition of wurtzite GaN, especially those modes correlated with longitudinal-optical (LO) phonons. Fig. 7 depicts the Raman spectra taken from the synthesized samples. No obvious scatterings are observed for the AlN film except that from the Si substrate. Besides those from the Si substrate, only the GaN-related Raman modes are observed for the GaN film and the $Al_xGa_{1-x}N$ films containing different Al compositions, as shown in Fig. 7. For the GaN film, two prominent Raman peaks appear at about 740 and 1485 cm^{-1}, which are attributed to the polar symmetry modes A_1(LO) and E_1(LO) and their overtones[37] (indicated by GaN LO and GaN 2LO in Fig. 7). In addition, a weak scattering near 575 cm^{-1} is resolved in the Raman spectrum of the GaN film, which can be assigned to the E_2 (high) mode of GaN. The one- and two-phonon scattering processes associated with the GaN A_1(LO) and E_1(LO) modes as well as with the GaN E_2 (high) mode are also observed for the films containing Al, but with an evident blue shift in vibration frequencies which increases as

the Al composition increases. This vibrational blue shift results from the incorporation of Al into the films. In addition, one can see a reduction in scattering intensity and a widening in scattering width with the increasing Al composition, also indicating the structure degeneration due to the Al incorporation.

TEM analysis was conducted to examine the crystalline structure of $Al_xGa_{1-x}N$ films grown on sapphire substrates. As a representative example, the results obtained for sample D before and after annealing are shown in Fig. 8. The bright-field TEM micrograph in Fig. 8(a) shows a dense structure of the 170 nm thick as-grown $Al_xGa_{1-x}N$ film. From the SAED pattern which was recorded from a circular area with 190 nm diameter (white circle in Fig. 8(a)) covering the layer cross-section and partially some glue used for TEM specimen preparation, it can be concluded that the as-grown $Al_xGa_{1-x}N$ film is of hexagonal wurtzite structure as displayed by the diffraction rings which were modeled using the software package JEMS (the inset of Fig. 8(a)). To display the $Al_xGa_{1-x}N$-sapphire interface quality, high-resolution TEM micrographs were taken, as shown in Fig. 8(b) and (d), particularly the bottom right insets. Evaluating the layer microstructure by Fourier transformation in direct vicinity to the interface hints that the growth of $Al_xGa_{1-x}N$ crystallites with preferred (0002) orientation parallel to the surface normal is discernable (top right inset in Fig. 8(b)). However, closer to the layer surface, the crystallites in the as-grown layer are more randomly distributed which is reflected in the SAED pattern in Fig. 8(a). Heat treatment of the sample leads to a sharpening of the texture relationship between the $Al_xGa_{1-x}N$ film and the sapphire substrate, as indicated by the diffractogram in the top right inset of Fig. 8(d). Additional reflections in the SAED pattern in Fig. 8(c) are due to the random growth of monoclinic Ga_2O_3 crystallites on the layer surface during annealing.

3.4 Optical properties and bandgap

The ternary $Al_xGa_{1-x}N$ films synthesized on sapphire substrates exhibit almost the same morphology and structure as those on Si substrates, so do the binary GaN and AlN films. The synthesized films on sapphire were then submitted for optical transmission measurements in the wavelength region ranging from 190 to 900 nm. All the films exhibit high transmittance in the visible and near IR regions, especially the AlN film which has a transmittance higher than 90% and whose transmission spectrum has a steep decline at around 220 nm with an absorption edge near 200 nm, as shown in Fig. 9. $Al_xGa_{1-x}N$ films B, C, and D have their absorption edges at about 350, 310 and 280 nm, respectively, located between the absorption edge of the AlN film and that of the GaN film as expected.

The absorption coefficient α can be determined from the recorded transmission spectra using $\alpha = -\ln(T)/t$ with film thickness t. The inset of Fig. 8 displays the relationship of $(\alpha h\nu)^2$ *versus* $h\nu$ near the bandgaps of these films, where $h\nu$ is the photon energy. It is obvious that these relationships show a linear dependence on $h\nu$ near the absorption edge, indicating the direct energy bandgaps of the synthesized films. By extrapolating the linear part of the $(\alpha h\nu)^2$ *versus* $h\nu$ plots to the photon energy axis, the bandgaps of samples A, B, C, D and E were calculated to

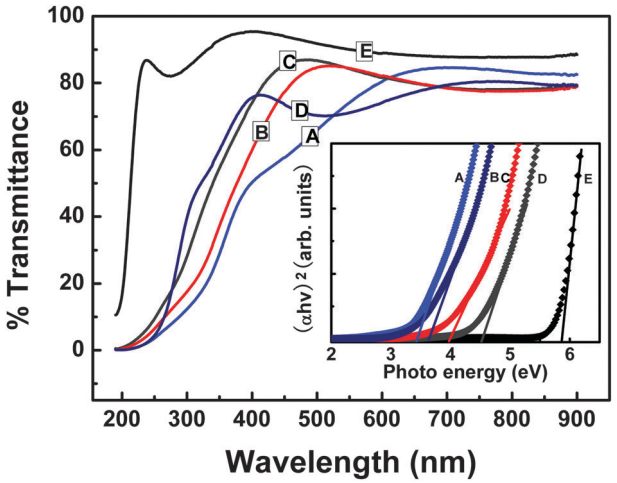

Fig. 9 Optical transmission spectra of samples A (A), B (B), C (C), D (D), and E (E) synthesized on sapphire substrates. The inset shows $(\alpha h\nu)^2$ *versus* $h\nu$ plots and their linear extrapolation for bandgap determination.

be 3.4, 3.6, 4.0, 4.5 and 5.9 eV, respectively, shifting toward the high-energy side with increasing x, with the calculated bandgap of AlN somewhat smaller than the reported value for AlN.[38,39]

The nonlinear dependence of the energy bandgap on the Al composition can be described by a parabolic form[40–43]

$$E_g(Al_xGa_{1-x}N) = xE_g(AlN) + (1 - x)\,E_g(GaN) - bx(1 - x) \quad (2)$$

where b is the bandgap bowing parameter, and $E_g(Al_xGa_{1-x}N)$, $E_g(AlN)$ and $E_g(GaN)$ are the bandgaps of $Al_xGa_{1-x}N$, AlN and GaN, respectively.

However, there is no consensus about the bowing parameter for $Al_xGa_{1-x}N$ alloys. The dispersion of bowing parameters reported in the literature extends from −0.8 eV (upward bowing) to +2.6 eV

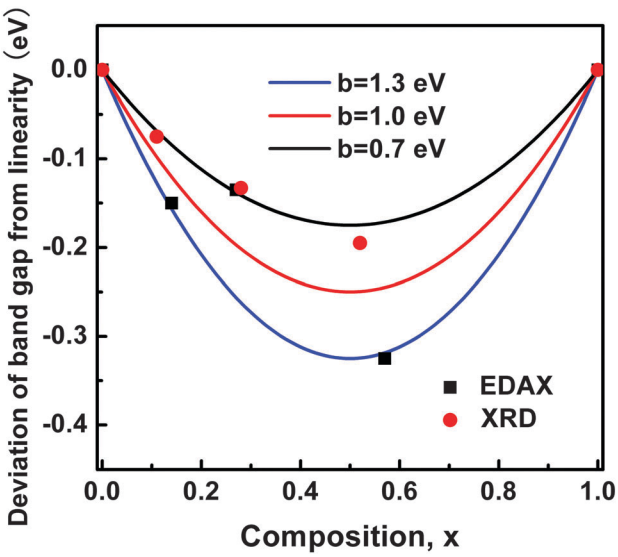

Fig. 10 Measured deviations of the bandgap from linearity with x for synthesized $Al_xGa_{1-x}N$ films. Solid reference lines show $-bx(1-x)$ with bowing parameters of 0.7, 1.0 and 1.3 eV.

(downward bowing).[41–44] Taking the calculated bandgap of GaN as E_g(GaN) = 3.4 eV and that of AlN as E_g(AlN) = 5.9 eV, we plot in Fig. 10 the deviations of the bandgap from linearity with x for $Al_xGa_{1-x}N$ obtained from the EDXS and XRD measurements and the parabolic compositional dependence. Here, the deviation of the bandgap from linearity is equal to $E_g(Al_xGa_{1-x}N) - xE_g(AlN) - (1 - x)\,E_g(GaN)$. It can be seen from Fig. 10 that all the data calculated whether from EDXS or from XRD in the present work lead to the bowing parameter locating between b = +0.7 and +1.3 eV. When using the lattice parameters calculated from XRD to determine the alloy compositions according to Vegard's law that the lattice parameters of $Al_xGa_{1-x}N$ vary linearly with x, we can see that the bowing parameter b is approximately 0.7 eV by comparing the deviation data, especially for $Al_xGa_{1-x}N$ with low Al compositions ($x < 0.5$). For high Al compositions ($x > 0.5$), the bandgap bowing parameter deviates slightly, tending to larger bandgap bowing.

4. Conclusions

In the reactive environment of nitrogen plasma generated by ECR discharge and with the assistance of the nitrogen plasma, ternary $Al_xGa_{1-x}N$ films were synthesized by the pulsed laser co-ablation of GaAs and Al targets and the variation of the Al composition was realized by simply varying the repetition rate of the pulsed laser beam ablating the Al target. The ternary $Al_xGa_{1-x}N$ films as well as binary GaN and AlN films appear with smooth surface and dense structure and are hexagonal wurtzite in crystal structure which tends to degenerate as the Al composition increases. The synthesized films show high optical transparency with the absorption edge of the $Al_xGa_{1-x}N$ films locating between those of GaN and AlN films. The bandgaps of the films having Al compositions x = 0, 0.11, 0.29, 0.52 and 1 were determined to be 3.4, 3.6, 4.0, 4.5 and 5.9 eV, respectively. The optical emission of the plasma generated by ECR discharge of N_2 gas and co-ablation of the GaAs and Al targets is rich in the emission bands of nitrogen molecules and molecular ions and the emission lines of aluminum, gallium and arsenic atoms and atomic ions. ECR discharge activated the N_2 gas and generated the reactive nitrogen plasma. The energetic Al and Ga atoms and ions ablated from the Al and GaAs targets traveled through the nitrogen plasma and reacted with the excited nitrogen species in the nitrogen plasma, forming $Al_xGa_{1-x}N$ precursors. The bombardment of the film surface by the low-energy plasma stream enhanced the formation of $Al_xGa_{1-x}N$ and the growth of $Al_xGa_{1-x}N$ films.

Acknowledgements

This work is supported by the National Natural Science Foundation of China (Contract No. 11275051) and the National Basic Research Program of China (Contract No. 2012CB934303). is also made to the Doctoral Fund of Chinese Ministry of Education (Contract No. 20110071110020).

Notes and references

1 F. A. Ponce and D. P. Bour, *Nature*, 1997, **386**, 351.
2 A. Khan, K. Balakrishnan and T. Katona, *Nat. Photonics*, 2008, **2**, 77.
3 T. Kuykendall, P. Ulrich, S. Aloni and P. Yang, *Nat. Mater.*, 2007, **6**, 951.
4 C. Y. He, Q. A. Wu, X. Z. Wang, Y. L. Zhang, L. J. Li, N. Liu, Y. Zhao, Y. N. Lu and Z. Hu, *ACS Nano*, 2011, **5**, 1291.
5 C. T. Yu, W. C. Lai, C. H. Yen and S. J. Chang, *Opt. Express*, 2014, **22**, 663.
6 M. Martens, J. Schlegel, P. Vogt, F. Brunner, R. Lossy, J. Wuerfl, M. Weyers and M. Kneissl, *Appl. Phys. Lett.*, 2011, **98**, 211114.
7 M. Moradi and P. Valizadeh, *J. Appl. Phys.*, 2011, **109**, 024509.
8 N. Rohrbaugh, I. Bryan, Z. Bryan, C. Arellano, R. Collazo and A. Ivanisevic, *Appl. Phys. Lett.*, 2014, **105**, 134103.
9 D. Christy, T. Egawa, Y. Yano, H. Tokunaga, H. Shimamura, Y. Yamaoka, A. Ubukata, T. Tabuchi and K. Matsumoto, *Appl. Phys. Express*, 2013, **6**, 026501.
10 V. P. Kladko, A. F. Kolomys, M. V. Slobodian, V. V. Strelchuk, V. G. Raycheva, A. E. Belyaev, S. S. Bukalov, H. Hardtdegen, V. A. Sydoruk, N. Klein and S. A. Vitusevich, *J. Appl. Phys.*, 2009, **105**, 063515.
11 T. Roy, Y. S. Puzyrev, B. R Tuttle, D. M. Fleetwood, R. D. Schrimpf, D. F. Brown, U. K. Mishra and S. T. Pantelides, *Appl. Phys. Lett.*, 2010, **96**, 133503.
12 K. Radhakrishnan, N. Dharmarasu, Z. Sun, S. Arulkumaran and G. I. Ng, *Appl. Phys. Lett.*, 2010, **97**, 232107.
13 J. C. Woicik, K. F. Ludwig and T. D. Moustakas, *Appl. Phys. Lett.*, 2012, **100**, 162105.
14 D. B. Chrisey and G. K. Hubler, *Pulsed Laser Deposition of Thin Films*, John Wiley and Sons, 1994.
15 R. Eason, *Pulsed Laser Deposition of Thin Films: Applications-Led Growth of Functional Materials*, John Wiley and Sons, 2007.
16 S. P. Lim, J. D. Long, S. Xu and K. Ostrikov, *J. Phys. D: Appl. Phys.*, 2007, **40**, 1085.
17 K. Ostrikov, E. C. Neyts and M. Meyyappan, *Adv. Phys.*, 2013, **62**, 113.
18 W. L. Wang, W. J. Yang, Z. L. Liu, Y. H. Lin, S. Z. Zhou, H. R. Qian, H. Y. Wang, Z. T. Lin, S. G. Zhang and G. Q. Li, *CrystEngComm*, 2014, **16**, 8500.
19 W. L. Wang, W. J. Yang, Z. L. Liu, Y. H. Lin, S. Z. Zhou, H. R. Qian, F. L. Gao and G. Q. Li, *CrystEngComm*, 2014, **16**, 4100.
20 H. Cai, Q. H. You, Z. G. Hu, S. Guo, X. Yang, J. Sun, N. Xu and J. D. Wu, *J. Alloys Compd.*, 2014, **616**, 137.
21 Y. Manabe and T. Mitsuyu, *J. Appl. Phys.*, 1988, **66**, 2475.
22 P. P. Liang, Y. L. Li, H. Cai, Q. H. You, X. Yang, F. L. Huang, J. Sun, N. Xu and J. D. Wu, *Spectrochim. Acta, Part B*, 2014, **101**, 226.
23 M. Losurdo, P. Capezzuto, G. Bruno, G. Leo and E. A. Irene, *J. Vac. Sci. Technol., A*, 1999, **17**, 2194.
24 N. Elkashef, R. S. Srinivasa, S. Major, K. P. Muthe and S. C. Sabharwal, *Thin Solid Films*, 1998, **333**, 9.
25 D. R. Lide, *CRC Handbook of Chemistry and Physics*, CRC Press, 85th edn, 2005.

26 J. Sun, A. M. Wu, N. Xu, Z. F. Ying, X. K. Shen, Z. B. Dong and J. D. Wu, *J. Vac. Sci. Technol., A*, 2005, **23**, 1633.
27 C. Ozgit-Akgun, E. Goldenberg, A. K. Okyay and N. Biyikli, *J. Mater. Chem. C*, 2014, **2**, 2123.
28 A. S. Hussein, S. M. Thahab, Z. Hassan, C. W. Chin, H. Abu Hassan and S. S. Ng, *J. Alloys Compd.*, 2009, **487**, 24.
29 A. R. Denton and N. W. Ashcroft, *Phys. Rev. A: At., Mol., Opt. Phys.*, 1991, **43**, 3161.
30 H. M. Tutuncu and G. P. Srivastava, *Phys. Rev. B: Condens. Matter Mater. Phys.*, 2000, **62**, 5028.
31 H. M. Tutuncu, G. P. Srivastava and S. Duman, *Physica B*, 2002, **316–317**, 190.
32 L. E. McNeil, M. Grimsditch and R. H. French, *J. Am. Ceram. Soc.*, 1993, **76**, 1132.
33 T. Prokofyeva, M. Seon, J. Vanbuskirk, M. Holtz, S. A. Nikishin, N. N. Faleev, H. Temkin and S. Zollner, *Phys. Rev. B: Condens. Matter Mater. Phys.*, 2001, **63**, 125313.
34 P. Wisniewski, W. Knap, J. P. Malzac, J. Camassel, M. D. Bremser, R. F. Davis and T. Suski, *Appl. Phys. Lett.*, 1998, **7**, 1760.
35 C. Bungaro, K. Rapcewicz and J. Bernholc, *Phys. Rev. B: Condens. Matter Mater. Phys.*, 2000, **61**, 6720.
36 V. Y. Davydov, I. N. Goncharuk, A. N. Smirnov, A. E. Nikolaev, W. V. Lundin, A. S. Usikov, A. A. Klochikhin, J. Aderhold, J. Graul, O. Semchinova and H. Harima, *Phys. Rev. B: Condens. Matter Mater. Phys.*, 2002, **65**, 125203.
37 P. Perlin, A. Polian and T. Suski, *Phys. Rev. B: Condens. Matter Mater. Phys.*, 1993, **47**, 2874.
38 W. M. Yim, E. J. Stofko, P. J. Zanzucchi, J. I. Pankove, M. Ettenberg and S. L. Gilbert, *J. Appl. Phys.*, 1973, **44**, 292.
39 P. B. Perry and R. F. Rutz, *Appl. Phys. Lett.*, 1978, **33**, 319.
40 D. Richardson and R. Hill, *J. Phys. C: Solid State Phys.*, 1972, **5**, 821.
41 S. R. Lee, A. F. Wright, M. H. Crawford, G. A. Petersen, J. Han and R. M. Biefeld, *Appl. Phys. Lett.*, 1999, **74**, 3344.
42 Y. Koide, H. Itoh, M. R. H. Khan, K. Hiramatu, N. Sawaki and I. Akasaki, *J. Appl. Phys.*, 1987, **61**, 4540.
43 M. Goano, E. Bellotti, E. Ghillino, C. Garetto, G. Ghione and K. F. Brennan, *J. Appl. Phys.*, 2000, **88**, 6476.
44 J. Wu, R. Palail, W. M. Jadwisienczak and M. S. Shur, *J. Phys. D: Appl. Phys.*, 2012, **45**, 015104.